Usherin is required for maintenance of retinal photoreceptors and normal development of cochlear hair cells

Xiaoqing Liu*, Oleg V. Bulgakov*, Keith N. Darrow†, Basil Pawlyk*, Michael Adamian*, M. Charles Liberman†, and Tiansen Li*‡

*Berman–Gund Laboratory for the Study of Retinal Degenerations and †Eaton–Peabody Laboratory, Harvard Medical School, Massachusetts Eye and Ear Infirmary, Boston, MA 02114

Edited by Jeremy Nathans, Johns Hopkins University School of Medicine, Baltimore, MD, and approved January 18, 2007 (received for review December 11, 2006)

Usher syndrome type IIA (USH2A), characterized by progressive photoreceptor degeneration and congenital moderate hearing loss, is the most common subtype of Usher syndrome. In this article, we show that the USH2A protein, also known as usherin, is an exceptionally large (≈600-kDa) matrix protein expressed specifically in retinal photoreceptors and developing cochlear hair cells. In mammalian photoreceptors, usherin is localized to a spatially restricted membrane microdomain at the apical inner segment recess that wraps around the connecting cilia, corresponding to the periciliary ridge complex described for amphibian photoreceptors. In sensory hair cells of the cochlea, it is associated transiently with the hair bundles during postnatal development. Targeted disruption of the *Ush2a* gene in mice leads to progressive photoreceptor degeneration and a moderate but nonprogressive hearing impairment, mimicking the visual and hearing deficits in USH2A patients. These data suggest that usherin is required for the long-term maintenance of retinal photoreceptors and for the development of cochlear hair cells. We propose a model in which usherin in photoreceptors is tethered via its C terminus to the plasma membrane and its large extracellular domain projecting into the periciliary matrix, where they may interact with the connecting cilium to fulfill important structural or signaling roles.

photoreceptor degeneration | retina | retinitis pigmentosa

Usher syndrome is the most frequent cause of combined deafness and blindness. Usher patients exhibit both sensorineural hearing defect and retinitis pigmentosa (RP), a progressive degeneration of the retinal photoreceptors (1, 2). Based on clinical features of the hearing defect, Usher syndrome is classified into three types: types I, II, and III (3). Usher syndrome type I (USH1) is the most severe form with profound congenital deafness and vestibular dysfunction. USH2 is characterized by moderate nonprogressive hearing loss without vestibular dysfunction and a tendency for more pronounced hearing loss for higher-frequency sounds. USH3 is distinguished from USH2 by the progressive nature of its hearing loss and occasional vestibular dysfunction. At least 10 mapped chromosomal loci and 8 genes now are known to be involved in the development of Usher syndrome (refs. 3 and 4; www.sph.uth.tmc.edu/Retnet).

USH2 accounts for well over one-half of all Usher cases (3, 5), and mutations in the *USH2A* gene are responsible for the majority of USH2 cases (5–9). In addition to typical USH2, a certain mutant allele of the *USH2A* gene also was found to cause nonsyndromic RP with little or no hearing defects (10). *USH2A* mutations were estimated to underlie ≈7% of all RP cases in North America, on a par with other major RP genes such as *RPGR* and rhodopsin (11). The product of the *USH2A* gene was designated usherin (8). Usherin transcript was originally reported to be 5 kb (5), encoding a putative protein of 170 kDa. This 170-kDa protein was predicted to be entirely extracellular, with motifs resembling common extracellular matrix proteins, and was described in several earlier studies (5, 12–14). A more recent study identified additional exons for the *USH2A* gene in the human genome, expanding the length of coding sequence to 15 kb (15), encoding a putative 600-kDa protein. In addition to the greatly expanded size, the recently identified exons also were predicted to encode a membrane-spanning segment followed by an intracellular PDZ-binding domain at the C terminus.

There have been conflicting reports about usherin tissue distribution and subcellular localization (4, 13, 16–18). The putative 600-kDa full-length protein never was confirmed from native tissues, and the function of usherin was poorly understood. It is interesting that usherin and no fewer than eight other Usher-related proteins specifically are required in both photoreceptor and cochlear hair cells, suggesting key functional or structural features shared between these two cell types. Indeed, both are ciliated sensory neurons. Photoreceptors possess a specialized photosensitive organelle known as the outer segment, a large modified cilium that is connected at its base to the cell body (inner segment) through a thin bridge called the connecting cilium. As the outer segment continuously is renewed, the connecting cilium has the vital role of trafficking nascent proteins to the outer segment. The analogous kinocilium of a cochlear hair cell appears transiently during development, when it is required for aligning the hair bundles (stereocilia) into the highly organized adult formation (3, 19). Stereocilia, also known as hair bundles, are mechanosensitive organelles required for displacement detection on a nanometer scale (20). Mutations affecting stereocilia formation and maintenance lead to deafness or Usher syndrome (16, 21–26). In addition, both types of sensory neurons also are characterized by ribbon synapses.

To investigate the molecular mechanism of usherin function *in vivo*, we carried out targeted disruption of the *Ush2a* gene in mice. Based on phenotype analysis of the *Ush2a*-null mice and analysis of usherin transcripts and proteins, we conclude that the dominant form of usherin in photoreceptors is the 600-kDa polypeptide as previously predicted (15). We propose that usherin function is related to the true cilia of the retinal photoreceptors and cochlear hair cells.

Author contributions: X.L. and T.L. designed research; X.L., O.V.B., K.N.D., B.P., M.A., and M.C.L. performed research; X.L., M.C.L., and T.L. analyzed data; and X.L. and T.L. wrote the paper.

The authors declare no conflict of interest.

This article is a PNAS direct submission.

Abbreviations: USH2A, Usher syndrome type II A; RP, retinitis pigmentosa; RPE, retinal pigment epithelium; immunoEM, immunoelectron microscopy; ERG, electroretinogram; GFAP, glial fibrillary acidic protein; DPOAE, distortion product otoacoustic emission.

Data deposition: The assembled murine usherin long variant sequence has been deposited in the GenBank database (accession no. DQ073638).

‡To whom correspondence should be addressed at: Massachusetts Eye and Ear Infirmary, 243 Charles Street, Boston, MA 02114. E-mail: tli@meei.harvard.edu.

This article contains supporting information online at www.pnas.org/cgi/content/full/0610950104/DC1.

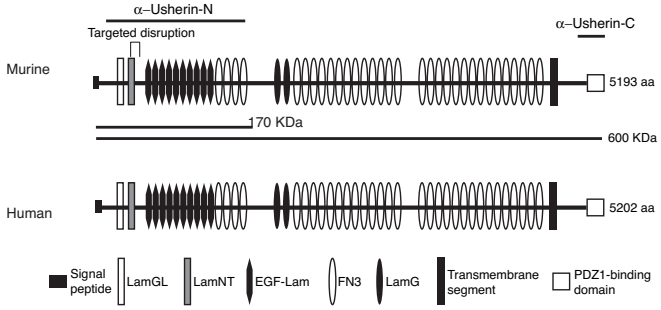

Fig. 1. Motif alignment of the murine and human usherins. Murine usherin shares 82% sequence identity and the same motif arrangement with its human ortholog. The lines (α-Usherin-N and α-Usherin-C) above the murine usherin sequence indicate the regions that were selected for making recombinant protein antigens. The two lines (170 kDa and 600 kDa) beneath the murine usherin sequence denote the two predicted usherin variants that had been reported. The site of targeted disruption encompassing exon 5 is indicated. Symbols representing different motifs are given at the bottom of the diagram. LamGL, LamG-like jellyroll fold domain; EGF-Lam, laminin-type epidermal growth factor-like domain; FN3, fibronectin type 3; LamG, laminin G domain.

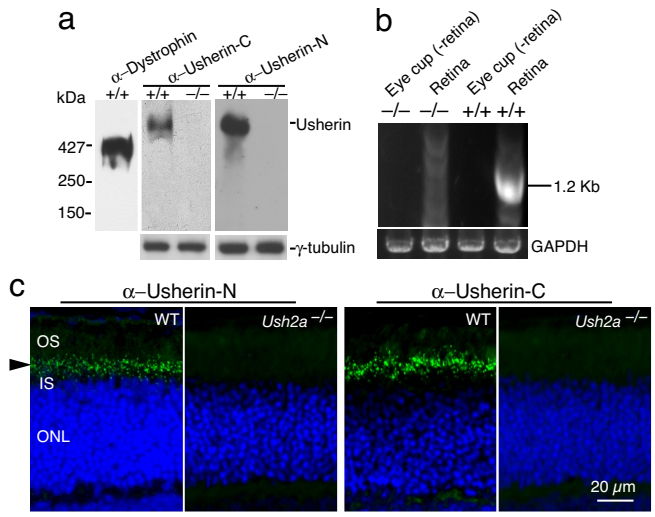

Fig. 2. Ablation of the *Ush2a* gene expression in mice. For details of targeting strategy, see supporting information (SI) *Methods*. (*a*) Immunoblotting run on agarose gels and probed by either α-Usherin-N and α-Usherin-C antibodies showed complete ablation of the long usherin variant (estimated at 600 kDa) in the homozygous mutant. Dystrophin from skeletal muscles was shown as a reference for molecular mass. The same samples run on a polyacrylamide gel and probed γ-tubulin served as a loading control. (*b*) RT-PCR analysis of WT tissues showed that usherin transcripts originated from the neural retina, not RPE cells. The expected 1.2-kb PCR product was absent from homozygous mutant tissues. (*c*) Immunofluorescence for usherin in the retina. In WT retinas, both α-Usherin-N and α-Usherin-C recognized a dotted staining (green) pattern between the inner and outer segment, indicative of the connecting cilia (arrowhead). In the *Ush2a*$^{-/-}$ retina, this staining pattern was missing. Nuclei were counterstained blue with Hoechst dye 33342. IS, inner segment; OS, outer segment; ONL, outer nuclear layer.

Results

Murine and Human Usherins Are Highly Conserved. By PCR amplification of murine retinal cDNA followed by DNA sequencing, both the long and short usherin variants previously reported were identified. The long usherin variant sequence was assembled from six overlapping fragments. The long murine *Ush2a* transcript is >15 kb in length, with an ORF of 5,193 aa codons (GenBank accession no. DQ073638). Its amino acid sequence is 82% identical to the long human usherin variant (5,202 aa) (Fig. 1). Murine and human usherin long variants have the same motif arrangement, with a large extracellular domain consisting of LamNT, EGF-Lam, LamGL, LamG, and FN3 motif repeats, a single membrane-spanning segment and a PDZ-binding C terminus predicted to reside intracellularly. Therefore, murine and human usherins are structurally highly conserved and likely to be functionally conserved as well.

The 600-kDa Long Usherin Variant Is the Predominant Form in Photoreceptor Cells. We ablated *Ush2a* gene expression in mice by targeted disruption (Fig. 2). We generated two antibodies against the N and C termini of the long usherin sequence. The N-terminal antibody was designed to recognize both the long and short variants, whereas the C-terminal antibody was specific for the long variant (Fig. 1). With these antibodies, immunoblotting revealed a protein band from retinal extracts migrating at an apparent molecular mass that was higher than dystrophin (427 kDa). This protein was completely ablated in *Ush2a*$^{-/-}$ retinas (Fig. 2*a*), identifying this protein as usherin. Its apparent molecular mass was consistent with the predicted size of 600 kDa for the usherin long variant. The 170-kDa short variant, however, was not detected by immunoblotting using the N-terminal antibody (Fig. 2*a*), which was generated with an antigen that overlapped with this putative 170-kDa isoform. This result does not rule out the presence of the shorter variant in the retina but does indicate that the long usherin variant is more abundant.

By RT-PCR analysis, usherin transcript was found expressed in the retina. To determine whether the transcript originated from the neural retina or from the retinal pigment epithelium (RPE), we performed RT-PCR analysis on dissected neural retinas and the posterior eye cup from which the neural retina had been removed. The latter tissue retained RPE. As shown in Fig. 2*b*, only the retina gave the expected usherin amplification product, indicating that usherin transcript was expressed primarily in the neural retina.

By using immunofluorescence, usherin was found in a region between the outer and inner segments of the photoreceptors (Fig. 2*c*). This is the region where the connecting cilia, which link the inner and outer segments, are aligned. The N- and C-terminal usherin antibodies gave an identical staining pattern, which was absent in the *Ush2a*$^{-/-}$ photoreceptors. Because the C-terminal antibody would recognize the long variant only, the identical staining patterns from the N- and C-terminal antibodies reinforce our conclusion that the long variant predominates in the retina. Usherin immunostaining was not present in the inner retina nor was it found in the RPE or the photoreceptor synapses as others have reported. These data suggest that usherin is expressed specifically in retinal photoreceptor cells.

Usherin Marks the Apical Inner Segment Recess That Wraps Around the Connecting Cilia. To determine usherin localization in photoreceptor cells more precisely, we carried out double-labeling immunofluorescence with well defined photoreceptor proteins that localized to this region, including RPGR, rootletin, and RP1 (Fig. 3*c*). RPGR is localized within the connecting cilia proper (27, 28). Rootletin, the structural constituent of the ciliary rootlet and separated from the connecting cilia only by a basal body, marks the proximal boundary of the connecting cilia (29). RP1, on the other hand, associates with the axonemal microtubules in the basal outer segments and marks the distal boundary of the connecting cilia (30, 31). Double labeling with these markers determined that usherin was distal to rootletin, proximal to RP1, and overlapped with RPGR (Fig. 3*a*).

Because usherin was predicted to be mostly extracellular, the above localization could be consistent with usherin's being tethered to the plasma membrane of the connecting cilia with its large extracellular domain projecting into the periciliary matrix. Equally plausible, however, was that usherin was tethered to the plasma

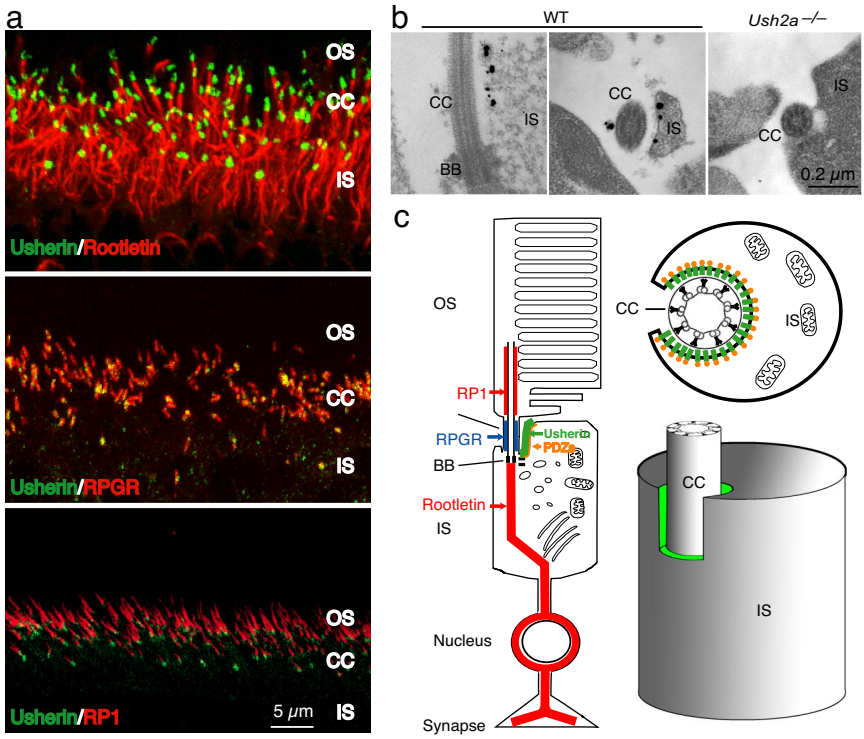

Fig. 3. Subcellular localization of usherin in the photoreceptors. (*a*) Double labeling of usherin (green) with markers (red) known to localize in or close to the connecting cilia. By using confocal microscopy, usherin was located just distal to the ciliary rootlet (*Top*), overlapping with RPGR (*Middle*), and proximal to RP1 (*Bottom*). (*b*) Ultrastructural localization of usherin in murine retina by immunoEM. In the WT photoreceptors, both longitudinal (*Left*) and cross-sectional (*Right*) views found immunogold labels (black dots) for usherin on the plasma membrane of the apical inner segment region that surrounded the cilium. In the *Ush2a*$^{-/-}$ photoreceptor (cross-sectional view), no gold labels were found. (*c*) A schematic representation of usherin localization in photoreceptors. A longitudinal profile of a photoreceptor in its entirety (*Left*), a cross-sectional view through the connecting cilium (*Upper Right*), and a 3D rendition of the photoreceptor inner segment in relation to the connecting cilium (*Lower Right*) are shown. Usherin is represented by the green color in all images. A PDZ domain protein (orange) is thought to interact with the C terminus (PDZ-binding motif) of usherin on the cytoplasmic side.

membrane in a specialized region at the apical inner segment that encircles the connecting cilia. The connecting cilia of photoreceptors sit in a recess formed by the invagination of apical inner segment plasma membrane. The narrow band of periciliary matrix materials separates the plasma membranes of the inner segment and of the connecting cilium. Usherin could be anchored via its C terminus to the plasma membrane of the cilium, the apical inner segment recess, or both. Immunofluorescence microscopy would not have sufficient resolution to distinguish between the two patterns of usherin localization. We therefore carried out immunoelectron microscopy (immunoEM) studies of usherin localization in photoreceptors. With the usherin C-terminal antibody, we found that usherin was associated exclusively with the plasma membrane of the apical inner segment recess (Fig. 3*b*). Based on these data, we propose a model in which usherin is tethered to the plasma membrane of the inner segment with its extracellular domain jutting into the periciliary matrix. Given its large size, usherin could readily come into contact and interact with the surface of the connecting cilium (Fig. 3*c*).

Usherin Is Essential for the Long-Term Maintenance of Photoreceptors. The postnatal development of retinal photoreceptors in the *Ush2a*$^{-/-}$ mice was indistinguishable from that of WT littermate controls as judged by histology and electroretinograms (ERGs) in younger mice. Up until 10 months of age, photoreceptor morphology, such as nuclear layer thicknesses or inner/outer segment lengths, was comparable to that of the controls as revealed by light and electron microscopy (data not shown), and ERGs were normal in the *Ush2a*$^{-/-}$ mice. That photoreceptors in the mutant were under stress was indicated by an up-regulation of glial fibrillary acidic protein (GFAP) in Müller cells in the predegenerating retinas. GFAP up-regulation is a nonspecific indicator of photoreceptor degeneration and typically precedes overt cell loss (32, 33). As mice grew older, additional signs of photoreceptor degeneration began to emerge in the mutant retinas. These signs included the gradual thinning of the photoreceptor nuclear layer and shortening of the inner/outer segments. By 20 months of age, more than one-half of the photoreceptors were lost, and the outer segments became very short and disorganized (Fig. 4*a*). Along with the loss of photoreceptors, ERG amplitudes declined so that by 20 months the a- and b-waves were reduced by >60% compared with those of age-matched WT controls (Fig. 4*b*). By immunofluorescence staining for cone opsins, we found that cone outer segments were severely shortened with cone opsins ectopically localizing to cell bodies (Fig. 4*c*), suggesting that cone photoreceptors also were undergoing degeneration. GFAP was found to be up-regulated from as early as 2 months of age (Fig. 4*c*) and remained so at the older ages (data not shown).

Usherin Deficiency Leads to Loss of Hair Cells and High-Frequency Threshold Elevation. To investigate the role of usherin in the inner ear, we immunostained the cochlear sensory epithelium for usherin, studied hair-cell morphology by scanning electron microscopy, and assessed cochlear function by measurement of distortion product otoacoustic emissions (DPOAEs). Usherin immunostaining in WT animals revealed expression in stereociliary bundles of both inner and outer hair cells but was absent in *Ush2a*$^{-/-}$ mice (Fig. 5*a*). The staining was strong at postnatal days 1–5 but was no longer detectable at 2 months of age (data not shown).

In common laboratory strains of mice, hearing is strongly

CELL BIOLOGY

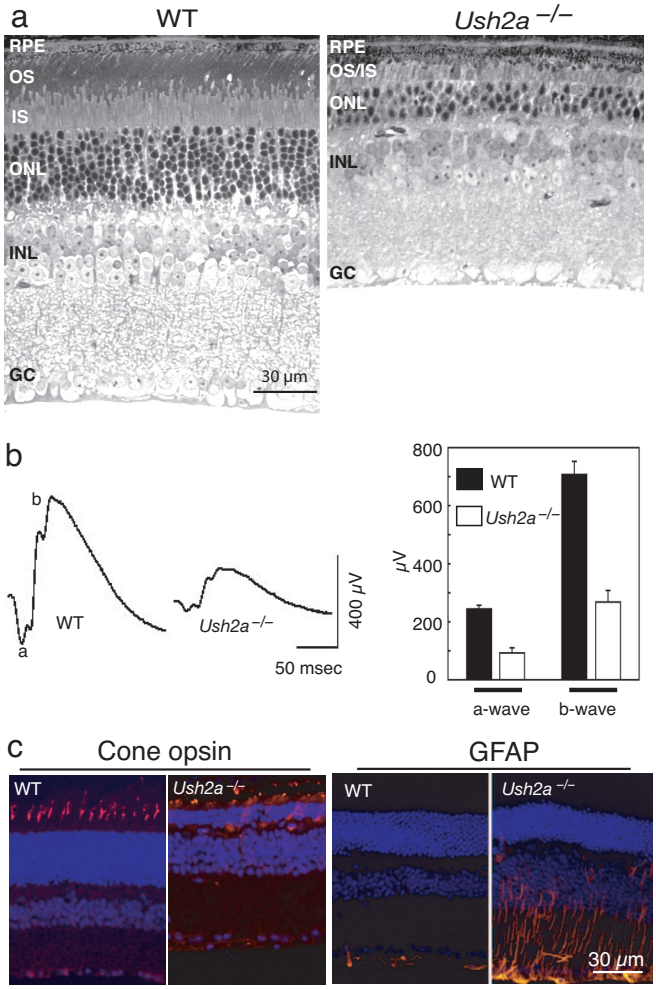

Fig. 4. Retinal degeneration in the *Ush2a*$^{-/-}$ mutant. (*a*) Light photomicrographs from an *Ush2a*$^{-/-}$ retina at the age of 20 months and an age-matched WT control are shown . The photoreceptor cell layer in the mutant was much thinner than that of the control. (*b*) Representative ERG tracings from a mutant at 20 months of age and an age-matched WT control are shown (*Left*). ERG data from a cohort of mutant and control mice are summarized (*Right*). Both the a- and b-wave amplitudes from the *Ush2a*$^{-/-}$ mutant ($n = 8$) were reduced significantly compared with the control ($n = 9$) ($P < 0.001$). OS, outer segment; IS, inner segment; ONL, outer nuclear layer; INL, inner nuclear layer; GC, retinal ganglion cells. (*c*) Immunofluorescence for cone opsins and GFAP in mutant and control mice. Cone opsin antibodies (mixed blue and green cone opsin antibodies) stained well organized cone outer segments in the WT retina but highlighted cell bodies and little outer segments in the mutant (at 20 months; *Left*). GFAP was up-regulated in the mutant (at 2 months; *Right*). Immunostaining signals are shown in orange. Cell nuclei are counterstained blue with Hoechst dye 33342.

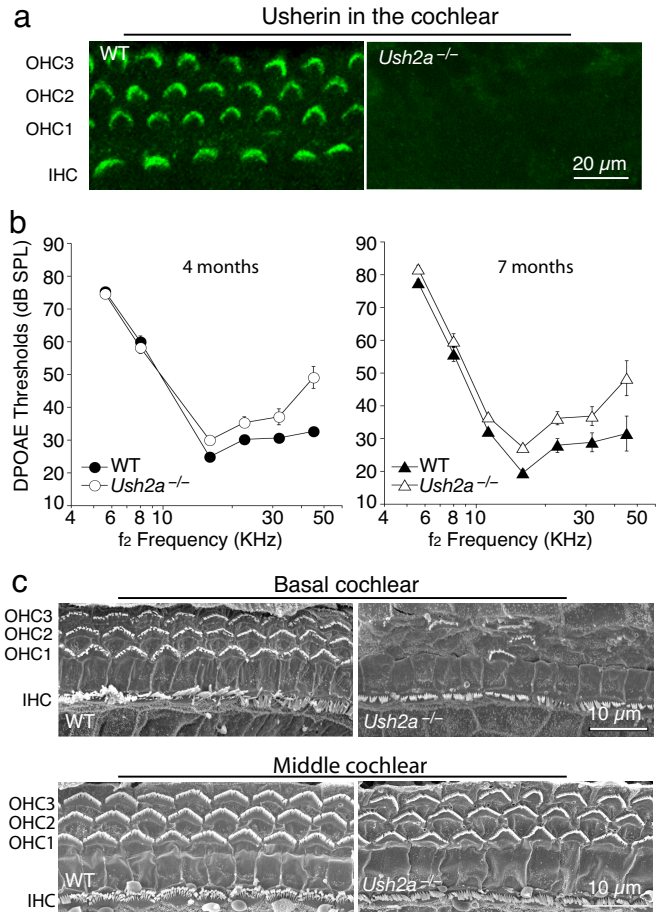

Fig. 5. The role of usherin in the inner ear. (*a*) Localization of usherin in the cochlea by immunofluorescence. Usherin staining in the WT (at postnatal day 1) shows an association with the hair bundles of inner hair cells (IHC) and the three rows of outer hair cells (OHC1, OHC2, and OHC3). Usherin was absent in the mutant. (*b*) Mean cochlear thresholds (±SEM) measured at 4 and 7 months by measurement of DPOAEs are shown. In each group, 20–24 ears (both ears from 10–12 animals) were tested. The difference between WT and *Ush2a*$^{-/-}$ mice was statistically significant ($P < 0.001$) for high-frequency sounds. Little difference between 4 months and 7 months for the *Ush2a*$^{-/-}$ ears was observed, indicating that the hearing loss is nonprogressive. (*c*) Ultrastructural changes in the cochlea by scanning electron microscopy. Basal and apical turns are shown. Many outer hair cells in the basal portion of the *Ush2a*$^{-/-}$ inner ear were missing, whereas those in the middle turn appeared normal, consistent with the observation that cochlear threshold shifts were more severe for high frequencies than for low frequencies. Inner hair cells were present throughout the cochlear spiral.

influenced by allelic variations in the cadherin 23 gene (*Cdh23*), particularly as they age (34). Our original mouse colony was homozygous for the hypomorphic allele (*Cdh23*^{753A}), a condition that leads to progressive, high-frequency hearing loss beyond 3 months of age (34). In our own preliminary hearing tests, we also saw effects from this allele, as indicated by subnormal response in a control group (data not shown). Thus, we embarked on a breeding scheme to remove the *Cdh23* hypomorphic allele (*Cdh23*^{753A}) from the *Ush2a* mutant line. We crossed the original *Ush2a*$^{-/-}$ mutant with the CBA/CaJ strain homozygous for the WT allele of *Cdh23* (*Cdh23*^{753G}). The F_1 offspring from this cross were *Ush2a*$^{+/-}$ and *Cdh23*$^{753A/753G}$. F_1 sibling mating produced several allelic combinations among the F_2 littermates. PCR amplification followed by DNA sequencing identified mice that were *Ush2a*$^{-/-}$; *Cdh23*$^{753G/753G}$ and mice that were *Ush2a*$^{+/+}$; *Cdh23*$^{753G/753G}$. These two groups of mice were enrolled for hearing tests as the mutant and control, respectively.

DPOAE measurements at 4 months of age showed normal cochlear function in the mutants at low frequency but a clear threshold elevation at higher test frequencies (Fig. 5*b*). Such observations are consistent with loss of outer hair cells in the cochlear basal turn. Threshold elevation had not progressed when the same cohort of mice was retested at 7 months of age (Fig. 5*b*). No head tilt, circling, or other obvious signs of vestibular dysfunction were observed in the *Ush2a*$^{-/-}$ mice. Thus, the *Ush2a*$^{-/-}$ phenotype is a nonprogressive moderate hearing loss resembling that seen in human USH2A patients.

Upon completion of the hearing tests, cochleas were processed for morphological examination. Scanning electron microscopy of the *Ush2a*$^{-/-}$ mice revealed normal hair-cell populations and

normal-appearing stereocilia bundles on both inner and outer hair cells throughout the apical half of the cochlea. In the basal turn, there was widespread loss of outer hair cells; however, the inner hair cells and their stereociliary bundles appeared normal (Fig. 5*c*).

Discussion

In this study, we generated and analyzed a mouse model in which all known variants of usherin were ablated. Usherin-null mice developed a spectrum of retinal and hearing defects closely resembling those of *USH2A* human patients, which include progressive photoreceptor degeneration and moderate, nonprogressive hearing loss, especially at higher frequencies. Interestingly, before this study, no genetic mouse model of Usher syndrome has been shown to develop overt photoreceptor degeneration. At least six mouse models with mutations in Usher syndrome genes, both engineered and naturally arisen, have been described. These include models for *USH1B* (myosin VIIA) (35–37), *USH1C* (harmonin) (38), *USH1D* (cadherin 23) (21, 39), and *USH1F* (protocadherin 15) (26), *USH1G* (sans) (40), and *USH2C* (very large G protein-coupled receptor 1) (41). Hearing defects in these models resembled those of the respective human conditions. However, none of these mouse models exhibited photoreceptor cell loss (42). The reason for the lack of photoreceptor degeneration in genetic murine models of Usher syndrome is unknown but may be because of functional redundancy in murine Usher genes or a very slow disease progression in the retina that makes it difficult to characterize. A recent study on mouse *Pcdh15* mutants shows that most of the mutant alleles affect exons that are alternatively spliced, suggesting removal of the affected exons could preserve some functional isoform of the gene product in the retina (43). It is not clear to what extent alternative splicing might explain the lack of overt retinal degeneration in other murine models of Usher syndrome. The *Ush2a*$^{-/-}$ mutant described here demonstrates overt photoreceptor degeneration in a mouse model of Usher syndrome. Photoreceptor degeneration in this model is slowly progressive, similar to RP in human patients. These data establish the *Ush2a*$^{-/-}$ mutant mouse as a valid model for Usher syndrome in terms of disease phenotype.

Two variants of usherin have been described in the literature based on genetic and biochemical studies (5, 13, 15). The short variant is predicted to be a secreted, extracellular protein, whereas the long variant is anchored on the cell membrane with a large extracellular domain and a short C-terminal PDZ-binding motif. Our study finds that the long variant of usherin, an exceptionally large protein of ≈600 kDa, is the predominant form in the retina. We further show that usherin localizes to a distinct region in the apical inner segment that forms a semiencircled recess and wraps around the connecting cilium. In frog photoreceptors, the plasma membrane over the inner segment is marked by a set of grooves and ridges visible by scanning EM and is termed the periciliary ridge complex (44). It has a 9-fold symmetry that apparently is correlated with the nine microtubule arrangements of the ciliary axoneme. Filaments were seen to bridge the top edges of the ridges. It is thought that the membrane microdomain marked by the periciliary ridge complex is a docking site for transport of proteins destined to the outer segments (44). In mammalian photoreceptors, a periciliary ridge complex is not apparent, perhaps because of the smaller size of the cell. It can be assumed, however, that a functional equivalent may exist. The spatially restricted distribution of usherin at this patch of plasma membrane marks it as a specialized microdomain and supports the view that a functional equivalent periciliary ridge complex does exist in mammals. Usherin is likely to be tethered via its C-terminal PDZ-binding motif to this membrane microdomain through protein–protein interaction with PDZ domain proteins (16–18) (see Fig. 3*c*) (unpublished observations). Plasma membranes covering the inner segments and the connecting cilium are <0.1 μm apart. Because of the large size of its extracellular domain, usherin can be envisioned as being anchored in the plasma membrane and interacting with surface proteins of adjacent membrane protrusions and/or with the surface of the connecting cilium. These interactions likely form the basis of usherin function in photoreceptor cells. Given that the initial development of *Ush2a*$^{-/-}$ retinas apparently is normal and that the photoreceptor phenotype is slowly progressive, we propose that usherin function is required in the long-term maintenance of photoreceptor cells.

Usherin also is localized to the stereocilia of cochlear hair cells but only in developing animals. In this study, we detected usherin expression in mouse pups at postnatal days 1–5 but not in young adults. Others have reported that usherin disappears from the cochlear hair cells around postnatal day 15 (16). This transient expression pattern of usherin is correlated temporally with the maturation of stereocilia and the disappearance of the kinocilia (45). Furthermore, our study indicates that the hearing loss in the usherin mutant mice is nonprogressive. Both the transient expression and the nonprogressive phenotype are consistent with usherin's having a role in the postnatal maturation of cochlear hair cells. Kinocilium in a hair cell is a true cilium and is the analogous structure to photoreceptor connecting cilium. Stereocilia, on the other hand, are not true cilia but are actin filament-based membrane protrusions. To some extent, they resemble the membranous protrusions constituting the periciliary ridge complex in photoreceptors. Kinocilia provide an important positional cue for the rotational alignment of stereociliary bundles. Once maturation of stereocilia is complete, the kinocilia in mammalian cochlear hair cells recede. It thus is likely that usherin participates in the interactions between the kinocilium and stereocilia and among stereocilia themselves during the period of dynamic changes in membrane topology on the hair-cell apical surface. The proposal that usherin is a component of the ankle links (16), which also appear transiently during postnatal development, is consistent with this view. As the kinocilium disappears, a functional requirement for usherin ceases. The role of usherin at least is partially redundant, because the hearing loss is moderate and confined to the higher frequency range and hair-cell degeneration is apparent only in the basal turn of the cochlea. In this regard, it is similar to VLGR1, another component of the ankle links (41). The loss of VLGR1 also leads to a hearing loss more pronounced in the higher-frequency range and disruption of cochlear hair cells confined to the basal half (41).

Other than the possession of a true cilium, another shared feature between photoreceptors and hair cells is the ribbon synapse. Others recently have proposed that usherin localizes and functions at the photoreceptor and hair-cell synapses, in conjunction with other Usher proteins (4, 17, 18). Our present study finds no evidence for the presence of usherin at the photoreceptor synapse or a defective synaptic transmission from photoreceptors to second-order retinal neurons. Therefore, our data argue against a significant function for usherin at the ribbon synapses. Usherin localizes to homologous membrane microdomains (stereocilia in hair cells and the mammalian equivalent of a periciliary ridge complex in photoreceptors) and putatively mediates the interaction between those structures and a true cilium. These interactions appear to fulfill important structural and signaling roles.

Materials and Methods

Generation of the *Ush2a* Knockout Mice. The murine *Ush2a* gene was disrupted by standard gene-targeting technique. The original *Ush2a* homozygotes we have generated (*Ush2a*$^{-/-}$) were homozygous for a cadherin 23 hypomorphic allele (*Cdh23*^{753A}) from their ancestral strains (C57BL/6 and 129 Sv). Because this hypomorphic allele would interfere with the hearing evaluation (34), the *Ush2a* mutant mice were crossed with CBA/CaJ, a strain with "gold standard" normal hearing (46), to generate Ush2a WT and knockout mice homozygous for the WT allele of Cdh23 (*Cdh23*^{753G}). For detailed targeting strategy, breeding scheme, and primer sequences used for amplification, see SI Fig. 6 and *SI Methods*.

Light and Electron Microscopy. Tissue processing and embedding into Epon resin for light microscopy were performed as described in ref. 29. ImmunoEM was performed with a preembedding method that used gold-conjugated secondary antibodies and silver enhancement. For detailed methods on immunoEM and scanning EM of the cochleas, see *SI Methods*.

Functional Tests for the Retina and Cochlea. ERG was performed to assess retinal function as described in ref. 47. DPOAE measurements were performed for evaluation of cochlear function as described in ref. 48.

Other Methods. Immunoblotting for usherin was carried out by using 1.2% agarose gels for separation because of its exceptionally large size. RT-PCR analysis and sequencing of the murine usherin coding region, generation of polyclonal usherin antibodies, and immunofluorescence were performed following previously described protocols (33). The chicken α-Usherin-N antibody and the rabbit α-Usherin-C antibody were used for this study. For detailed methods, see *SI Methods*.

We thank Norman Michaud and Akella Sreedevi for histology and confocal microscopy support; Leslie Liberman for dissection of inner ear cochleas; Scott Adams for DNA sequencing; Xun Sun for GFAP immunostaining; Eric Pierce for RP1 antibody; and Drs. Eliot Berson, Thaddeus Dryja, and Michael Sandberg for helpful discussions. This work was supported by National Institutes of Health Grants R01 EY10309, R01 DC00188, and P30 DC05209; the Foundation Fighting Blindness; and National Institutes of Health Core Grant for Vision Research P30 EY14104.

1. Beaty TH, Boughman JA (1986) *Am J Med Genet* 24:493–504.
2. Boughman JA, Vernon M, Shaver KA (1983) *J Chronic Dis* 36:595–603.
3. Petit C (2001) *Annu Rev Genomics Hum Genet* 2:271–297.
4. Reiners J, Nagel-Wolfrum K, Jurgens K, Marker T, Wolfrum U (2006) *Exp Eye Res* 83:97–119.
5. Eudy JD, Weston MD, Yao S, Hoover DM, Rehm HL, Ma-Edmonds M, Yan D, Ahmad I, Cheng JJ, Ayuso C, *et al*. (1998) *Science* 280:1753–1757.
6. Kimberling WJ, Weston MD, Moller C, van Aarem A, Cremers CW, Sumegi J, Ing PS, Connolly C, Martini A, Milani M, *et al*. (1995) *Am J Hum Genet* 56:216–223.
7. Dreyer B, Tranebjaerg L, Rosenberg T, Weston MD, Kimberling WJ, Nilssen O (2000) *Eur J Hum Genet* 8:500–506.
8. Weston MD, Eudy JD, Fujita S, Yao S, Usami S, Cremers C, Greenberg J, Ramesar R, Martini A, Moller C, *et al*. (2000) *Am J Hum Genet* 66:1199–1210.
9. Pennings RJ, Te Brinke H, Weston MD, Claassen A, Orten DJ, Weekamp H, Van Aarem A, Huygen PL, Deutman AF, Hoefsloot LH, *et al*. (2004) *Hum Mutat* 24:185.
10. Rivolta C, Sweklo EA, Berson EL, Dryja TP (2000) *Am J Hum Genet* 66:1975–1978.
11. Seyedahmadi BJ, Rivolta C, Keene JA, Berson EL, Dryja TP (2004) *Exp Eye Res* 79:167–173.
12. Huang D, Eudy JD, Uzvolgyi E, Davis JR, Talmadge CB, Pretto D, Weston MD, Lehman JE, Zhou M, Seemayer TA, *et al*. (2002) *Genomics* 80:195–203.
13. Bhattacharya G, Miller C, Kimberling WJ, Jablonski MM, Cosgrove D (2002) *Hear Res* 163:1–11.
14. Pearsall N, Bhattacharya G, Wisecarver J, Adams J, Cosgrove D, Kimberling W (2002) *Hear Res* 174:55–63.
15. van Wijk E, Pennings RJ, te Brinke H, Claassen A, Yntema HG, Hoefsloot LH, Cremers FP, Cremers CW, Kremer H (2004) *Am J Hum Genet* 74:738–744.
16. Adato A, Lefevre G, Delprat B, Michel V, Michalski N, Chardenoux S, Weil D, El-Amraoui A, Petit C (2005) *Hum Mol Genet* 14:3921–3932.
17. Reiners J, van Wijk E, Marker T, Zimmermann U, Jurgens K, te Brinke H, Overlack N, Roepman R, Knipper M, Kremer H, Wolfrum U (2005) *Hum Mol Genet* 14:3933–3943.
18. van Wijk E, van der Zwaag B, Peters T, Zimmermann U, Te Brinke H, Kersten FF, Marker T, Aller E, Hoefsloot LH, Cremers CW, *et al*. (2006) *Hum Mol Genet* 15:751–765.
19. Denman-Johnson K, Forge A (1999) *J Neurocytol* 28:821–835.
20. Schneider ME, Belyantseva IA, Azevedo RB, Kachar B (2002) *Nature* 418:837–838.
21. Siemens J, Lillo C, Dumont RA, Reynolds A, Williams DS, Gillespie PG, Muller U (2004) *Nature* 428:950–955.
22. Boeda B, El-Amraoui A, Bahloul A, Goodyear R, Daviet L, Blanchard S, Perfettini I, Fath KR, Shorte S, Reiners J, *et al*. (2002) *EMBO J* 21:6689–6699.
23. Bolz H, von Brederlow B, Ramirez A, Bryda EC, Kutsche K, Nothwang HG, Seeliger M, del C-Salcedo Cabrera M, Vila MC, Molina OP, *et al*. (2001) *Nat Genet* 27:108–112.
24. Verpy E, Leibovici M, Zwaenepoel I, Liu XZ, Gal A, Salem N, Mansour A, Blanchard S, Kobayashi I, Keats BJ, *et al*. (2000) *Nat Genet* 26:51–55.
25. Sollner C, Rauch GJ, Siemens J, Geisler R, Schuster SC, Muller U, Nicolson T (2004) *Nature* 428:955–959.
26. Alagramam KN, Murcia CL, Kwon HY, Pawlowski KS, Wright CG, Woychik RP (2001) *Nat Genet* 27:99–102.
27. Hong DH, Yue G, Adamian M, Li T (2001) *J Biol Chem* 276:12091–12099.
28. Hagstrom SA, Adamian M, Scimeca M, Pawlyk BS, Yue G, Li T (2001) *Invest Ophthalmol Vis Sci* 42:1955–1962.
29. Yang J, Liu X, Yue G, Adamian M, Bulgakov O, Li T (2002) *J Cell Biol* 159:431–440.
30. Liu Q, Zhou J, Daiger SP, Farber DB, Heckenlively JR, Smith JE, Sullivan LS, Zuo J, Milam AH, Pierce EA (2002) *Invest Ophthalmol Vis Sci* 43:22–32.
31. Hong DH, Pawlyk B, Sokolov M, Strissel KJ, Yang J, Tulloch B, Wright AF, Arshavsky VY, Li T (2003) *Invest Ophthalmol Vis Sci* 44:2413–2421.
32. Hong DH, Pawlyk BS, Shang J, Sandberg MA, Berson EL, Li T (2000) *Proc Natl Acad Sci USA* 97:3649–3654.
33. Liu X, Bulgakov OV, Wen XH, Woodruff ML, Pawlyk B, Yang J, Fain GL, Sandberg MA, Makino CL, Li T (2004) *Proc Natl Acad Sci USA* 101:13903–13908.
34. Noben-Trauth K, Zheng QY, Johnson KR (2003) *Nat Genet* 35:21–23.
35. Gibson F, Walsh J, Mburu P, Varela A, Brown KA, Antonio M, Beisel KW, Steel KP, Brown SDM (1995) *Nature* 374:62–64.
36. Lillo C, Kitamoto J, Liu X, Quint E, Steel KP, Williams DS (2003) *Adv Exp Med Biol* 533:143–150.
37. Gibbs D, Kitamoto J, Williams DS (2003) *Proc Natl Acad Sci USA* 100:6481–6486.
38. Johnson KR, Gagnon LH, Webb LS, Peters LL, Hawes NL, Chang B, Zheng QY (2003) *Hum Mol Genet* 12:3075–3086.
39. Di Palma F, Holme RH, Bryda EC, Belyantseva IA, Pellegrino R, Kachar B, Steel KP, Noben-Trauth K (2001) *Nat Genet* 27:103–107.
40. Kikkawa Y, Shitara H, Wakana S, Kohara Y, Takada T, Okamoto M, Taya C, Kamiya K, Yoshikawa Y, Tokano H, *et al*. (2003) *Hum Mol Genet* 12:453–461.
41. McGee J, Goodyear RJ, McMillan DR, Stauffer EA, Holt JR, Locke KG, Birch DG, Legan PK, White PC, Walsh EJ, Richardson GP (2006) *J Neurosci* 26:6543–6553.
42. Ahmed ZM, Riazuddin S, Riazuddin S, Wilcox ER (2003) *Clin Genet* 63:431–444.
43. Haywood-Watson RJ, II, Ahmed ZM, Kjellstrom S, Bush RA, Takada Y, Hampton LL, Battey JF, Sieving PA, Friedman TB (2006) *Invest Ophthalmol Vis Sci* 47:3074–3084.
44. Peters KR, Palade GE, Schneider BG, Papermaster DS (1983) *J Cell Biol* 96:265–276.
45. Lim DJ, Anniko M (1985) *Acta Otolaryngol Suppl* 422:1–69.
46. Gao J, Wu X, Zuo J (2004) *Brain Res Mol Brain Res* 132:192–207.
47. Li T, Sandberg MA, Pawlyk BS, Rosner B, Hayes KC, Dryja TP, Berson EL (1998) *Proc Natl Acad Sci* 95:11933–11938.
48. Kujawa SG, Liberman MC (2006) *J Neurosci* 26:2115–2123.